13th World Conference on Earthquake Engineering
Vancouver, B.C., Canada
August 1-6, 2004
Paper No. 1119

SHAKE TABLE TESTS OF REINFORCED CONCRETE FLAT PLATE FRAMES AND POST-TENSIONED FLAT PLATE FRAMES

Thomas H.-K. KANG [1], and John W. WALLACE [2]

SUMMARY

A research study was undertaken to assess performance of flat plate systems constructed with slab shear reinforcement under dynamic loads. The research program consisted of shake table tests and accompanying analytical studies of two, approximately one-third scale, two-story, two-bay, slab-column frames. One specimen was constructed with reinforced concrete (RC) slab, whereas the other specimen consisted of post-tensioned (PT) slab. The shear capacity of the slab-column connections was enhanced by the use of stud-rails for both specimens. Lateral drift ratios of approximately 3% and 4% were achieved during testing for the RC and PT frames, respectively, with relatively little loss of lateral load capacity. Although slab-column punching failures occurred for both specimens, the degree of damage observed was limited compared with tests on specimens without shear reinforcement under slowly varying loads. Good agreement between analytical and experimental results was achieved by using an innovative modeling approach.

INTRODUCTION

Design practice on the west coast of the US has evolved such that the lateral strength and stiffness are provided with either a perimeter frame or a core wall, or both (dual system). A slab-column frame is commonly used to support gravity loads. The slab-column frame is checked for deformation compatibility to ensure it can undergo the design lateral drift associated with the lateral system without loss of gravity load carrying capacity. Continuous slab bottom reinforcement is provided through the column to protect against progressive collapse (i.e., support of gravity loads after punching failure); therefore, it is plausible that some designers assume that deformation compatibility requirements are satisfied a priori. A substantial short-coming of this assumption exists, that is, the possibility that punching failures may occur at a displacement level that is substantially less than that for the design displacement. Code changes have been approved by ACI Committee 318 to clarify and simplify the deformation compatibility check for the 2005 ACI 318 code. These provisions will be discussed later.

For a more comprehensive analysis of deformation compatibility requirements of slab-column frames, or where slab-column frames are used to resist lateral loads (e.g., Zone 2), it is necessary to model the lateral

[1] Graduate Research Assistant, Department of Civil & Environmental Engineering, University of California, Los Angeles, USA
[2] Associate Professor, Department of Civil & Environmental Engineering, University of California, Los Angeles, USA

load response. A common approach is to use an effective slab width to represent the flexural stiffness of the slab, where the three-dimensional system is modeled as a two-dimensional frame using an effective slab with thickness h and width of αl_2 and a conventional column model. The α-factor is derived using elastic plate theory to result in an effective slab width with uniform rotation that yields the same rotational stiffness as the original system with non-uniform rotation (Pecknold [1]). The α-value for the effective beam width model depends primarily on the column and slab aspect ratios, whereas the influence of cracking on stiffness is accounted for by using an additional factor, commonly referred to as a β-factor (Moehle and Diebold [2]).

For flat plate floor systems, shear (V_u) and unbalanced moment (M_{unb}) from the slab are assumed to be transferred to the column by: (1) direct shear and eccentric shear acting on a critical section within the slab adjacent to the column perimeter (Fig. 1(a)), and (2) slab flexural yielding within a slab transfer width of c_2+3h centered on the column (Fig. 1(b)). The portion of the unbalanced moment resisted by flexure over the slab transfer width of c_2+3h and by eccentric shear, as well as the nominal shear strength capacity of the slab critical section (V_n), are typically determined using ACI 318-02 [3] requirements. The maximum shear stress on the slab critical section is a sum of the direct shear stress and the maximum shear stress due to eccentric shear (Fig. 1(a)). If the connection strength is insufficient to transfer the unbalanced moment (i.e., $V_u > \phi V_n$ anywhere on the slab critical section), then a punching shear failure is assumed to occur. The shear strength of the slab-column connection can be increased by using either a drop panel or slab shear reinforcement. Currently, use of slab shear reinforcement in the form of stud-rails is popular.

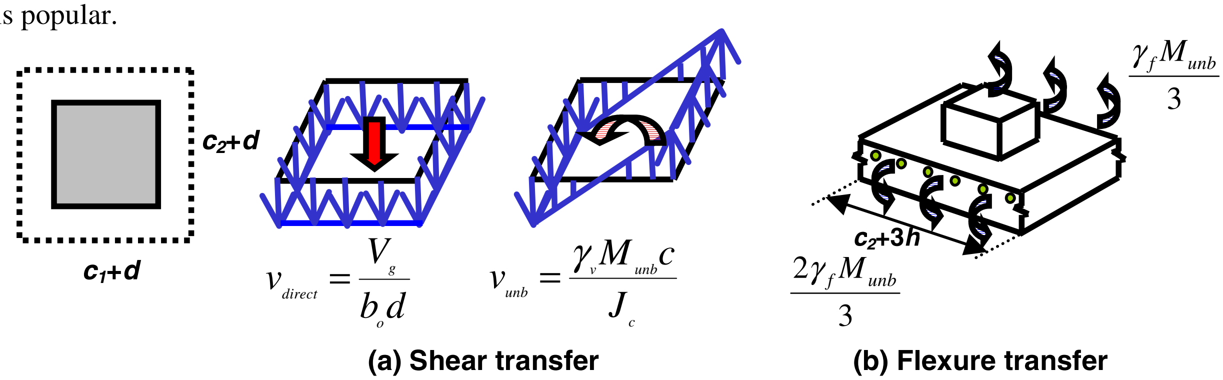

Figure 1 Direct shear and unbalanced moment transfer.

A number of experimental studies have been conducted to assess the lateral load behavior of flat plate systems (e.g., Hawkins and Michelle [4], Robertson and Durrani [5], Moehle [6]). A review of test results from these studies indicates that the shear strength of the slab critical section decreases as the lateral drift increases and that the magnitude of the gravity shear stress ($V_u/b_o d$) on the slab critical section around the column perimeter significantly influences the drift level at which a connection punching failure occurs. For gravity shear stress ratios greater than 0.4, evaluation of test results indicates that little displacement ductility capacity exists prior to punching failure; therefore, ACI 318-02 [3] places a limit of $0.4\phi V_n$ on the concrete shear strength of the critical section (S21.12.6.8), where ϕV_n is taken equal to ϕV_c if no shear reinforcement is used.

Use of post-tensioned slab-column systems with stud-rail shear reinforcement has become a very popular system for supporting gravity loads, as use of post-tensioning allows for relatively long spans and the use of stud-rails (shear reinforcement) enables the use of relatively thin slabs (and avoids the use of drop panels). The existing data for slab-column connections are limited primarily to tests of isolated, conventionally reinforced slab-column connections both with and without shear reinforcement (see Robertson et al. [7]). Very limited tests have been conducted on post-tensioned specimens subjected to cyclic loading, and no tests have been conducted for dynamic loadings or for post-tensioned systems with shear reinforcement. Given that the use of flat plate systems with slab shear reinforcement at the slab-column connections, in particular, post-tensioned systems, has become increasingly popular, shake table tests of two, approximately one-third scale slab-column frames were undertaken to address these gaps.

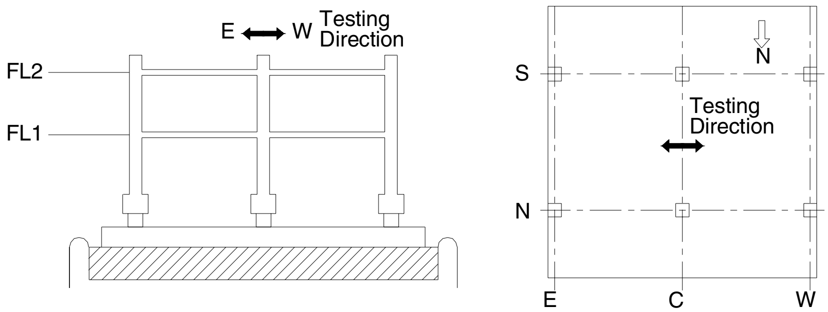

Figure 2 Test specimen on shake table.

Figure 3 RC slab reinforcement. (a) Overview. (b) Interior connection.

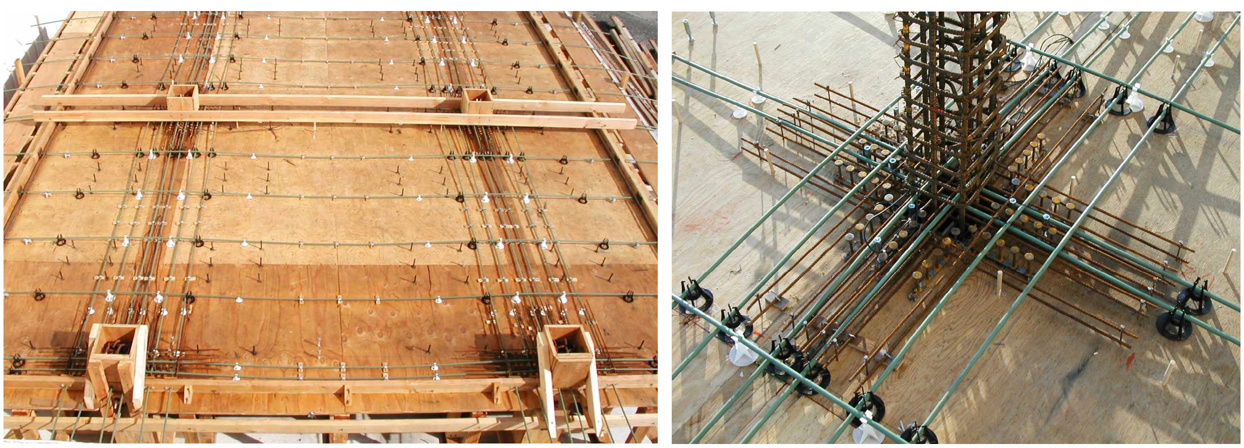

Figure 4 PT slab reinforcement. (a) Overview. (b) Interior connection.

OVERVIEW OF SHAKE TABLE TESTS

Two, approximately one-third scale replicas of a reinforced-concrete (RC) flat plate system and a post-tensioned (PT) flat plate system, were constructed and tested at the UC Berkeley Richmond Field Station. Each specimen consisted of a 2×2 bay slab-column frame, two stories high (Fig. 2). An overview of the designs, instrumentation, and testing of the specimens is provided in the following sections.

Specimen design and construction
Plan views and slab reinforcement are shown in Fig. 3 and 4. For the RC specimen, a span length of 2.06 m and a slab thickness of 89 mm were used, whereas 2.84 m spans and a 76.2 mm thick slab were used for the PT specimen. The resulting slab span-to-depth ratios of 23.1 (RC) and 37.3 (PT) are close to typical values used for RC (25 to 30) and PT (40 to 45) construction. Columns cross sections were 203 mm x 203 mm reinforced with 8 – 12.7 mm diameter longitudinal bars with a nominal yield stress of 414 MPa. Design concrete compressive strength was 27.6 MPa. Slab reinforcement for the RC and PT specimens consisted of 9.5 mm and 6.35 mm diameter bars, respectively, whereas post-tensioning consisted of 7.94 mm nominal diameter, seven wire strand with an ultimate strength of 1,725 MPa. The gravity shear ratio for the interior connections was 0.25 and 0.29 for the design concrete strength of f'_c = 27.6 MPa for the RC and PT specimens, respectively. Shear reinforcement, in the form of stud-rails, was used to increase the nominal shear strength of the slab-column connections. The specimens were designed such that yielding of slab flexural reinforcement was expected prior to shear failure within the shear reinforced region of the slab-column connections. Detailed information including measured material properties are presented by Kang et al. [8].

Instrumentation and testing
During testing, information was collected from 192 channels for each specimen. A detailed accounting of the instrumentation used is provided by Kang et al. [8]. The instrumentation layout was selected to allow the determination of important response quantities such as: story shears and overturning moments, story displacements and accelerations, rebar and stud-rail strains, and slab and column moments and curvatures, with a particular emphasis on evaluating unbalanced moment transfer at slab-column connections during the dynamic tests.

Table 1 Testing sequence and table motion characteristics.

RC Specimen						PT Specimen					
ID	*PHA*	I_A	*D*	T_p	T_m	ID	*PHA*	I_A	*D*	T_p	T_m
Free Vibration Tests 1 & 2 (FV 1 & 2)						Free Vibration Tests 1 & 2 (FV 1 & 2)					
Run 1	0.109	12.7	7.9	0.290	0.307	Run 1	0.095	10.2	8.8	0.318	0.320
R 2-1	0.287	89.2	11.3	0.438	0.295	Run 2	0.276	77.7	8.9	0.346	0.363
Free Vibration Tests 3 & 4 (FV 3 & 4)						Free Vibration Tests 3 & 4 (FV 3 & 4)					
R 2-2	0.256	94.2	11.3	0.439	0.286	Run 3	0.413	202	11.0	0.407	0.408
Free Vibration Tests 5 & 6 (FV 5 & 6)						Free Vibration Tests 5 & 6 (FV 5 & 6)					
Run 3	0.407	224	10.9	0.438	0.319	Run 4	1.144	1730	9.9	0.558	0.518
Free Vibration Tests 7 & 8 (FV 7 & 8)						Free Vibration Tests 7 & 8 (FV 7 & 8)					
Run 4	1.254	1775	9.9	0.439	0.366	Run 5	1.275	2221	9.8	0.585	0.552
Free Vibration Tests 9 & 10 (FV 9 & 10)						Free Vibration Tests 9 & 10 (FV 9 & 10)					

Note: *PHA* = Peak horizontal acceleration [g]; I_A = Arias intensity [cm/sec] (see Kramer [9], pp. 82).
D = Time interval between the points at which 5 % and 75% of the Arias intensity has been recorded [sec].
T_p = predominant period [sec]; T_m = mean period [sec].

The specimens (Fig. 5(a)) were subjected to several runs of uniaxial shaking, with the intensity of shaking increased for each subsequent run. A ground motion with fairly long duration and without significant near-fault effects was used, the CHY087W record from the 21 September 1999 Taiwan earthquake. The record was time-compressed by $1/\sqrt{3}$ to account for the dimensional scale factor. The accelerations of the record ground motion were modified to provide increasing intensity for subsequent tests as indicated in Table 1.

EXPERIMENTAL RESULTS AND ANALYTICAL MODELING

Results of free vibration tests

Free vibration testing was conduced prior to shake table testing and after each shake table test to assess changes in stiffness and damping of the specimens (Table 2). During the free vibration tests, the shake table platform was blocked, ensuring that the table was fixed and hydraulic actuators under the table did not affect dynamic properties of the test structures. The natural damped fundamental period (T_n) was determined by averaging the time between response peaks for several cycles and dividing by the number of cycles for 17 and 15 channels for the RC and PT frames, respectively. Damping ratios (ζ) were determined using the logarithmic decrement method. Fourier amplitude spectra of the response histories obtained during the free vibration tests also were used to identify first and second mode periods (T_{p1}, T_{p2}). As anticipated, periods and damping ratios increased as the testing sequence progressed, with the most significant increases noted for Run 4 for the RC specimen.

Table 2 Summary of free vibration tests.

RC	T_n [sec]	ΔT_n	T_{p1} [sec]	ΔT_{p1}	T_{p2} [sec]	ΔT_{p2}	ζ	$\Delta\zeta$
FV 1, 2	0.233	-	0.240	-	0.057	-	0.0119	-
FV 3, 4	0.285	22%	0.308	28%	0.071	25%	0.0323	171%
FV 5, 6	0.293	3%	0.319	4%	0.076	7%	0.0311	-4%
FV 7, 8	0.318	9%	0.334	5%	0.075	-1%	0.0394	27%
FV 9,10	0.481	51%	0.566	69%	0.113	51%	0.0608	54%
PT	T_n [sec]	ΔT_n	T_{p1} [sec]	ΔT_{p1}	T_{p2} [sec]	ΔT_{p2}	ζ	$\Delta\zeta$
FV 1, 2	0.276	-	0.286	-	0.071	-	0.0163	-
FV 3, 4	0.305	11%	0.315	10%	0.074	4%	0.0213	31%
FV 5, 6	0.333	9%	0.336	7%	0.076	3%	0.0339	59%
FV 7, 8	0.432	30%	0.444	32%	0.096	26%	0.0419	24%
FV 9,10	0.465	8%	0.502	13%	0.105	9%	0.0503	20%

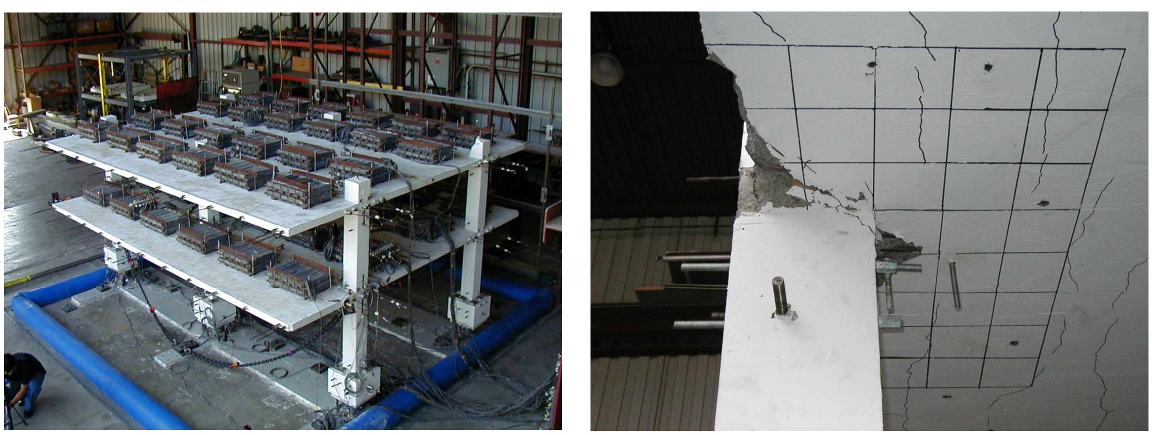

Figure 5 (a) PT specimen overview. (b) Punched connection (RC specimen).

Observed Damage

Significant cracking was observed both on the top and bottom of the slabs adjacent to the column; however, in general, cracks were not observed outside the shear-reinforced region for the RC specimen. The most significant slab damage was observed at the exterior connections of the RC specimen where substantial "torsional cracking" and concrete spalling occurred during Run 4 (Fig. 5(b)). For the PT specimen, less severe cracking was observed in the connection regions; however, cracking was observed at the exterior connections outside of the region reinforced with the banded post-tensioning. As well, yield lines were observed to extend the full width of the slab for the PT specimen. Overall, the damage observed at the RC connections was more significant and more widely distributed than damage observed for the PT specimen.

Significant relative rotation between the slabs and the columns was observed during Run 4 for both the RC and PT specimens, indicating that moment transfer strength at some connections had been lost, that is, a hinge had formed and the connection was free to rotate. Inspection of the connections (using a hammer to tap the concrete) also indicated that connection damage had occurred.

Linear behavior and modeling

Displacement transducers were used to obtain the relative displacement between floor slab levels and the column footing, which were corrected to account for the lateral displacement due to rotation of the column footings. Base shear forces were measured from tri-axial load cells as well as derived from floor acceleration records multiplied by the floor mass (details provided by Kang [10]). Average responses obtained for the two frames (frames N and S in Fig. 1) are plotted in Fig. 6(a) and 6(b) for Run 2-2 (RC) and Run 2 (PT), respectively. Peak roof displacements were in the range of 6.5 to 12.5 mm, and the measured responses show modest nonlinear response.

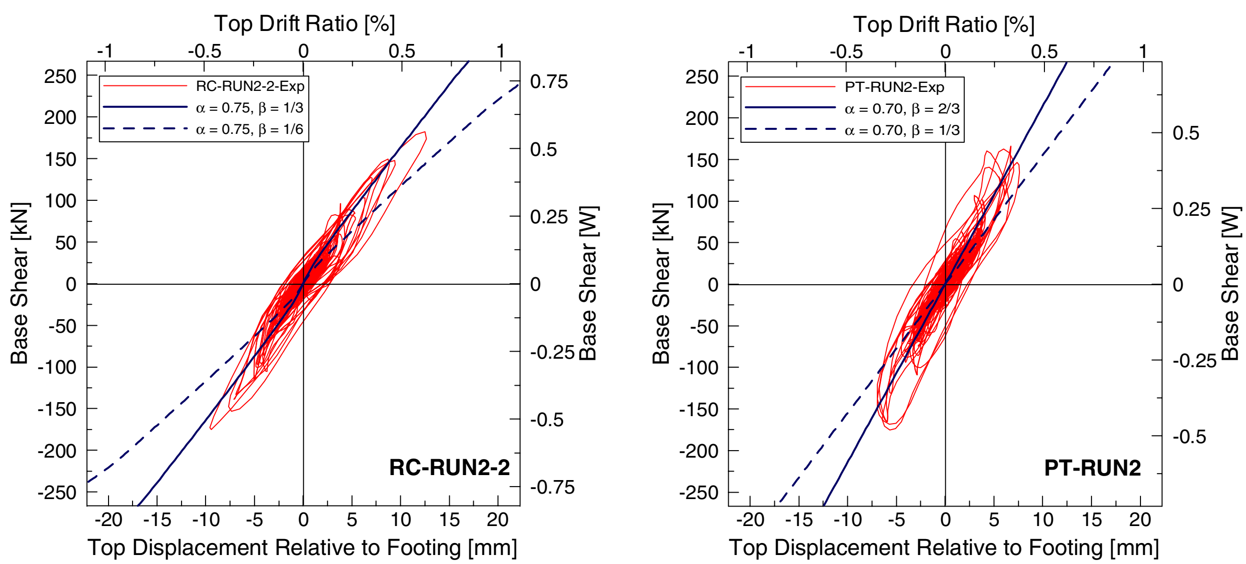

Figure 6 **Base shear versus top relative displacement (a) RC-Run 2-2. (b) PT-Run 2.**

Analytical models were created for each specimen to allow comparison of responses obtained with analytical models with responses obtained during the tests. Responses for Runs 1 and 2 (or 2-2) for each specimen were compared to determine appropriate α- and β-factors for the effective slab width model. The structure was modeled using the OpenSees platform [11] as a plane frame as shown in Fig. 7. A fiber model, with the material properties based on results obtained in material testing, was used for the columns. The dependence of column stiffness on column axial load is considered directly using a fiber model. Rotational springs with a spring constant of 5,650 kN-m/rad were included in the model at the base of column footings to account for footing rotation and to allow direct comparison between experimental and analytical results.

Appropriate values of α and β were determined by varying modeling parameters and comparing analytical and experimental responses. Values for α were determined using the free vibration test results prior to Run 1 (i.e., prior to conducting shake table tests), whereas values for β where determined using results for Run 2. Predominant periods determined from the analytical models for Run 1 for the RC specimen were 0.233 and 0.240 sec for α-values of 0.75 and 0.5, respectively, indicating that the fundamental period of the model was insensitive to changes in the α-value. Analytical results for the PT specimen indicated that the fundamental period was more sensitive to changes in the α-value, as the predominant period increased from 0.271 to 0.315 sec for α-values of 0.75 and 0.5, respectively. Fundamental periods of the models were matched with fundamental periods determined from the experimental results to obtain α-values of approximately 0.75 and 0.70 for the RC and PT specimens, respectively.

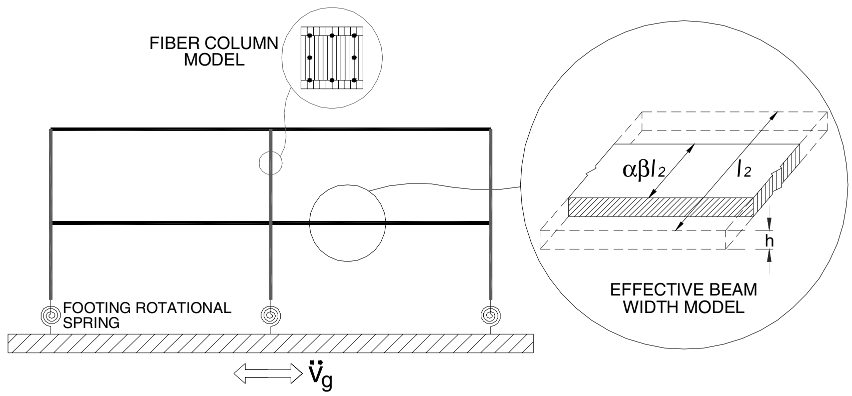

Figure 7 Plane frame modeling.

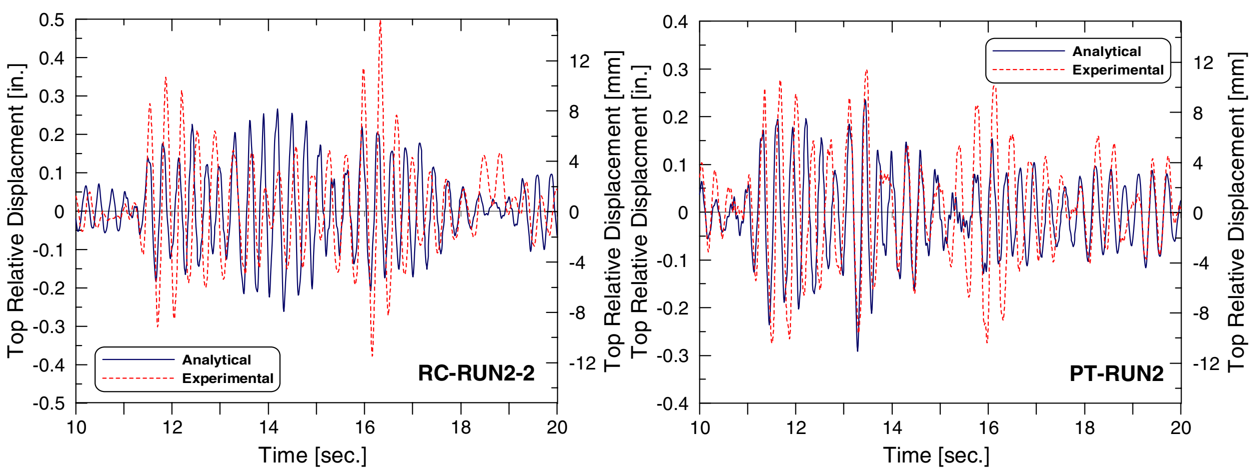

Figure 8 Response Histories. (a) RC-Run 2-2. (b) PT-Run 2.

Responses of the test structures to Run 2-2 (RC) or Run 2 (PT) were used to assess the reduction of slab stiffness due to cracking by comparing the relative stiffness for these runs with results for the free vibration tests prior to testing. Given the α-factors of 0.75 and 0.70 for the RC and PT specimens determined from the free vibration testing, respectively, β-values of approximately 1/3 and 2/3 resulted in good agreement between experimental and analytical determined periods. Push-over analyses were conducted to compare analytical results using the α (RC: 0.75, PT: 0.70) and β (RC: 1/3, PT: 2/3) values determined with experimentally obtained results (Fig. 6). Results presented in Fig. 6 indicate that the values used for α and β capture the load versus displacement response of the systems tested reasonably well. Table 3 presents comparisons of the α-factors obtained for the RC and PT specimens with various recommended values. The results obtained in this study are quite close to the values recommended in FEMA-274 [12].

Response history analyses of the RC and PT models with the same α- and β-values noted in the previous paragraph were conducted and computed responses are compared to experimental results in Fig. 8. Portions of the response histories compare favorably for the RC specimen (Fig. 8(a)), although the peak values are not well represented, where as results for the PT specimen compare quite well. The discrepancy between the RC and PT comparisons may be due to the influence of footing rotations, which were measured directly for the PT specimen whereas footing rotations were calculated indirectly for the RC specimen using results from the PT specimen test.

Table 3 Effective beam width factor - α.

	RC Specimen		PT Specimen	
Measured - α	0.75		0.70	
	$\alpha_{Theoretical}$	$\alpha_{Theoretical} / \alpha_{Measured}$	$\alpha_{Theoretical}$	$\alpha_{Theoretical} / \alpha_{Measured}$
Pecknold [1]	0.78	1.04	0.71	1.01
Allen et al. [13]	0.57	0.76	0.57	0.81
FEMA-274 [12]	0.74	0.99	0.61	0.87

Nonlinear behavior and modeling

In the preceding section, results derived from the experiment were compared to results obtained from analytical models for low-to-moderate levels of shaking, where essentially elastic behavior was anticipated. For greater intensity shaking, nonlinear responses were observed (Fig. 9), including yielding of slab reinforcement, yielding at column bases, and punching at slab-column connections; therefore, more comprehensive models are needed to capture the nonlinear behavior.

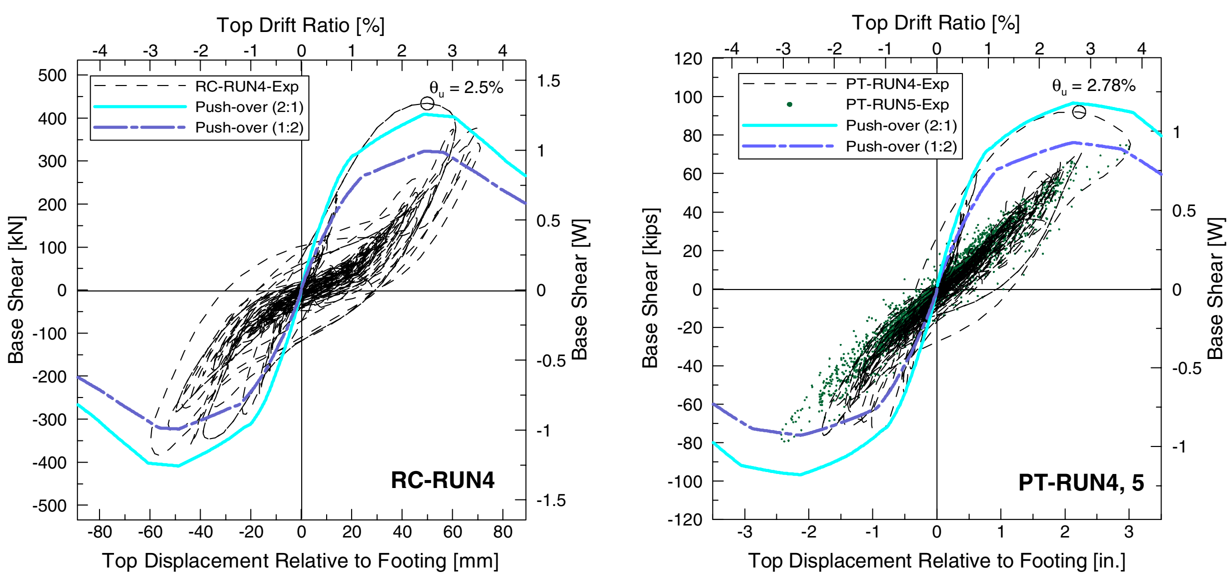

Figure 9 Base shear versus top relative displacement (a) RC-Run 4. (b) PT-Run 4 & 5.

Experimental results of base shear versus top relative displacement

Base shear versus top displacement histories are presented in Fig. 9 for Run 4 (RC), and Run 4 and 5 (PT). The RC specimen was subjected to peak drift levels of approximately 3% with only moderate strength deterioration. The measured base shear of the RC specimen began to degrade after t = 12.68 sec, when the top drift ratio reached 2.5% (Fig. 9(a)). The peak value of top drift of 2.78% occurred at t = 11.08 sec for the PT specimen, and strength deterioration was observed for lateral drifts exceeding approximately 3% (Fig. 9(b)). Results for the RC specimen reveal significant pinching of the hysteresis loops relative to the PT specimen. The loss of stiffness due to punching of the slab-column connections is apparent for both specimens.

The hysteresis loops for the lateral load versus top displacement relation for the PT specimen are narrower than the corresponding loops for the RC specimen. For the PT specimen, after yielding of the nominal quantity of bonded slab reinforcement occurred, the PT specimen acts as an essentially elastic structure with very low stiffness due to the presence of the unbonded post-tensioning reinforcement. This behavior is apparent in Run 5, as the stiffness of the initial cycles of Run 5 match closely the stiffness for cycles at the end of Run 4. More detailed assessment of punching failures and drift capacities at punching are provided by Kang and Wallace [14], [15].

Analytical modeling – Nonlinear responses

Initial member properties for the nonlinear model were adopted directly from the linear model, that is, an effective slab width of $\alpha\beta l_2$ used for the "slab" beams framing between columns and a fiber column model. Given the concentration of nonlinear responses at the slab-column connections, more detailed modeling approaches were needed to capture yield of reinforcement and punching. These approaches are summarized in the following paragraphs.

Nonlinear behavior due to yielding of slab reinforcement within the column strip or within the slab transfer width of c_2+3h adjacent to the slab-column connections was modeled as shown in Fig. 10(a), where flexural yielding can occur within the column strip or due to unbalanced moment within a connection element. Punching failures are expected to occur either when the shear capacity of the slab critical section is reached or when drift capacities of the slab-column connections are reached for a given gravity shear ratio. Specific attributes of the modeling approach adopted are described in the following items.

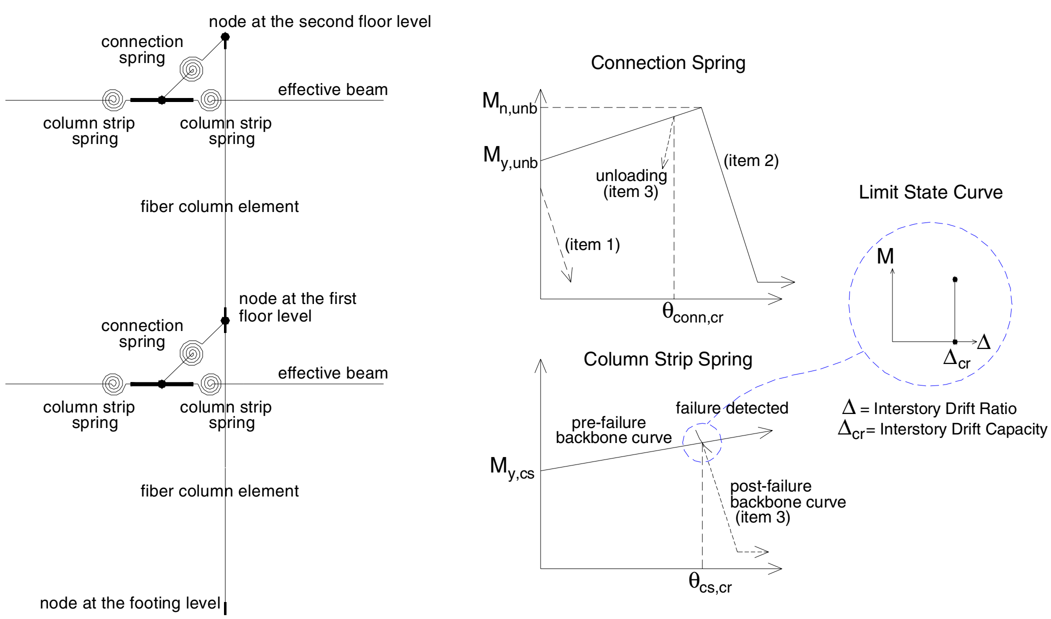

(a) Slab-column modeling. (b) Rigid plastic spring. (c) Limit state curve.

Figure 10 Nonlinear modeling.

1. <u>Punching failure prior to yielding of slab flexural reinforcement</u> (item 1, Fig. 10(b))

Punching failure occurs when the sum of direct gravity shear stress and shear stress induced by a fraction of unbalanced moment transferred by eccentric shear reaches to shear stress capacity on the slab critical section, that is:

$$v_u = \frac{V_g}{b_o d} \pm \frac{\gamma_v M_{unb} c}{J_c} \geq v_n \tag{1}$$

where V_g is the gravity force to be transferred from the slab to the column, b_o is the perimeter of critical section, d is the effective slab depth, γ_v is the fraction of unbalanced moment transferred by eccentric shear, M_{unb} is the unbalanced moment, c is the distance from the centroid of the critical section to the perimeter of the critical section that results in the smallest value of M_{unb} (or the largest shear stress), J_c is the polar moment of inertia of the critical section, and v_n is the nominal shear capacity at the connection. The nominal shear strength on the critical section within the shear reinforced region is $v_n = v_c + v_s$, whereas the nominal shear strength for the critical section outside the shear reinforced zone is $v_n = v_c$.

For this case, the capacity of the connection spring drops suddenly prior to reaching yield, as shown in Fig. 10(b) (item 1). It is noted that the test specimens were designed such that yielding of slab reinforcement was expected to occur prior to punching failure (see items 2 and 3).

2. Yielding of slab reinforcement followed by punching failure (item 2, Fig. 10(b))
The capacity to transfer unbalanced moment from the slab to the column was modeled using a rigid plastic (connection) spring as shown in Fig. 10(b). The yield capacity for unbalanced moment transfer of the connection element ($M_{y,unb}$ in Fig. 10(b)) is determined such that yielding of the slab reinforcement within the transfer width of c_2+3h occurs. After the yield capacity of the connection spring is reached, additional moment transfer at the slab-column connection exists as residual capacity exists to transfer moment by eccentric shear (since punching failure has not occurred); therefore, additional moment is transferred only by eccentric shear (i.e., $\gamma_f = 0$ and $\gamma_v = 1$ after reaching the $M_{y,c+3h}$). The nominal capacity of the connection spring to transfer unbalanced moment ($M_{n,unb}$ in Fig. 10(b)) is set equal to the unbalanced moment that exhausts the ability of the connection to transfer moment by eccentric shear. Punching failure of the connection is possible prior to reaching $M_{n,unb}$ if the slab rotation at the connection (determined as the average rotation for the slabs framing into an interior connection) reaches a critical value as described in item 3.

For the RC specimen, yielding of the connection spring is expected to occur prior to yield of the slab reinforcement with the column strip. For the PT specimen, since tendons are banded and essentially all of the bonded reinforcement is within c_2+3h, slab flexural yielding is modeled only by using a column strip spring, such that failure modes of the PT specimen are determined as either item 1 or item 3.

3. Punching failure after flexural yielding within the column strip (item 3, Fig. 10(b))
Flexural yielding in the slab adjacent to the slab-column connection is considered on either side of an interior connection or on one side of an exterior connection by using column strip springs. Punching failure is modeled by assuming the moment capacity of the slab drops to a residual (e.g., zero) capacity once a critical story drift ratio is reached (item 3, Fig. 10(b)). The critical story drift ratio is detected by using a limit state model (Elwood [16]), as discussed in the following paragraph. The yield capacity of the column strip spring ($M_{y,cs}$) is modeled separately from the nominal capacity of the connection spring ($M_{n,unb}$), such that punching failure can result from either reaching a limiting story drift for a given gravity shear ratio (reaching the limit state) or reaching the capacity of the connection spring (eccentric shear failure).

Limit state model
Elwood [16] developed a limit state model to initiate strength degradation after reaching a defined limit state. His original work focused on column shear strength; however, the model is ideally suited for detecting punching at slab-column connections. For slab-column connections, the limit state surface can be defined using inter-story drift. Once the failure-identifying parameter (i.e., story drift ratio) reaches the limit state surface (that is, reaches a prescribed drift limit for a given gravity shear ratio), a punching

failure is "detected" and the ability of the slab-column connection to transfer moment (or unbalanced moment) degrades according to a specified backbone relation and degradation parameters. The limit state model simplifies modeling of punching failures, as plastic rotations due to yielding of either the connection spring and/or the column strip spring are incorporated into story drift ratios and monitored throughout the analysis; therefore, defining a critical rotation at failure is not necessary. In this study, the story drift demands (Fig. 10(c)) were defined based on the experimental results of top (RC: 2.5%, PT: 2.78%) and second story (RC: 3.12%, PT: 4.02%) drift ratios at punching for the connections at the first and second floor levels, respectively (Kang and Wallace [15]).

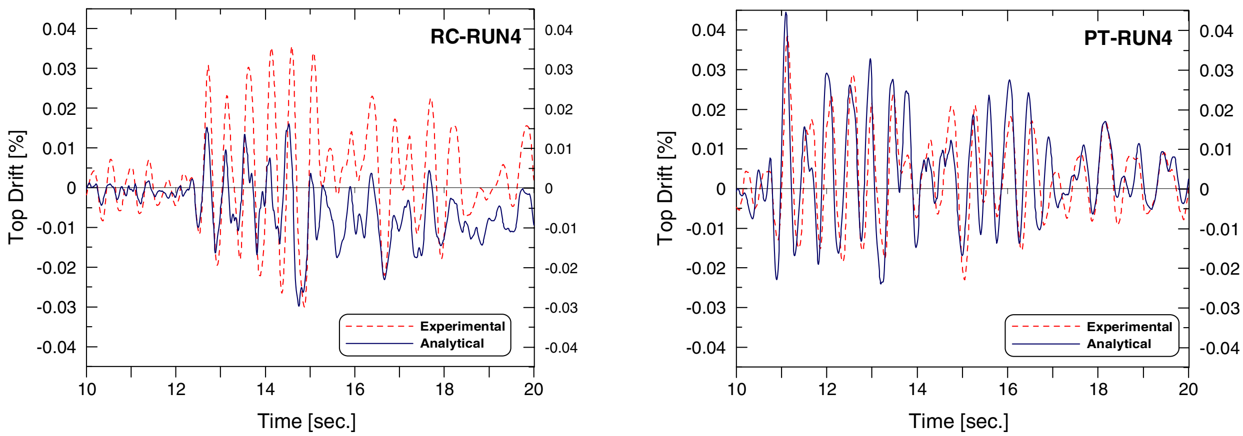

Figure 11 Response Histories. (a) RC-Run 4. (b) PT-Run 4.

Preliminary model results

Preliminary nonlinear analysis results are presented for static push-over and dynamic response history analyses, as shown in Fig. 9 and 11. The push-over curves plotted in Fig. 9 were computed for force ratios at the first and second floor levels of 2:1 and 1:2, respectively. The results are consistent with prior findings (Moehle and Diebold [2]), that is, the results indicate that a ratio of story forces of 2:1 yields better results within the linear range whereas a ratio of 1:2 yields better results within the nonlinear range.

Test results are plotted for Run 4 (RC) or Runs 4 and 5 (PT), to allow comparison for significant nonlinear responses. The push-over relations for the RC (Fig. 9(a)) and PT (Fig. 9(b)) specimens compare quite well with the response envelope for the test results. The response history results shown in Fig. 11 indicate that period and peak values compare favorably well, especially for the PT specimen. Results for the RC specimen show significant differences between measured and predicted values for positive displacement.

PUNCHING FAILURE AND DRIFT CAPACITY AT PUNCHING

Punching Failure

For isolated connections tested under static, monotonically increasing loads for each applied load or drift cycle, it is relatively easy to determine when connection punching occurs, as the lateral load capacity of the specimen experiences a sudden drop. In contrast, for dynamic tests of frame systems under simulated earthquake loading, the specimen undergoes continuous loading and unloading; therefore, a more detailed evaluation is required to assess when punching failures occur. In this study, slab and column curvatures were compared to determine if punching failure occurred.

When punching failure occurs, the slab loses its ability to transfer moment from the slab to the column; therefore, one approach to assessing if connection punching occurred is to plot the relationship between slab curvature and column curvature. As slab curvature increases, the column curvature should either increase or remain approximately constant if the slab has yielded, unless slab moment capacity drops (i.e., punching occurs) or the column yields. Column yielding is not expected since the columns of the two specimens were designed to be stronger than the slab; therefore, for this study, a drop in column curvature when significant slab curvatures exist signals that the strength deterioration is occurring at the slab-column connection (i.e., punching failure).

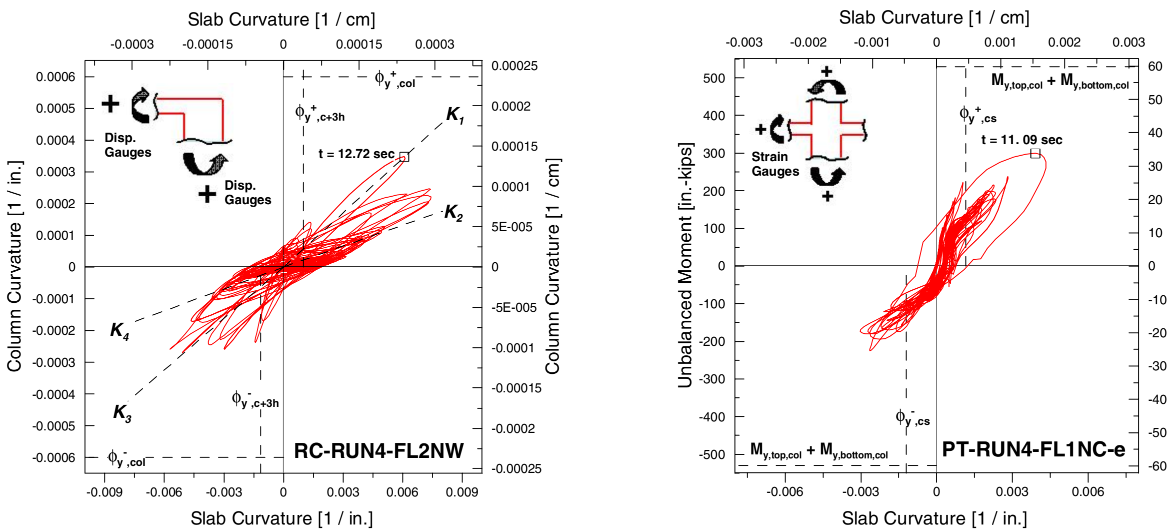

Figure 12 Curvature diagrams. (a) RC-FL2NW. (b) PT-FL1NC-e

Slab curvature versus column curvature (or unbalanced moment) relations were determined for all connections; however, only representative results are presented here for the exterior roof level connection of the RC specimen (Fig. 12(a)), the interior floor level connection of the PT specimen (Fig. 12(b)). Calculated yield curvatures for the slab and column are also indicated on these figures as broken lines. As shown in Fig. 12(a), for positive curvatures, column curvatures begin to drop for higher slab curvatures, indicating that the moment transfer capacity of the slab-column connection is degrading, which is consistent with punching failure. Therefore, the results indicate that a punching failure occurred for FL2NW connection of the RC specimen between t = 12.71 and 12.73 sec for Run 4. The ratio of column curvature to slab curvature (K_1) at a significant positive peak (t = 12.72 sec) is 0.057, thereafter reduces to K_2 = 0.022 at t = 30.35 sec. The smaller value of K_2 relative to K_1 is a result of a punching failure. For negative bending, column curvature remains relatively constant at 0.0001/cm for a large range of slab curvatures (0.00004 to 0.00025/cm), indicating that the slab has yielding, but no degradation in the strength of the slab-column connection has occurred. However, degradation of the column curvature appears to initiate at approximately t = 14.38 sec with K_3 = 0.054, versus K_4 = 0.023 at t = 30.06 sec.

At the first story interior connection (PT-FL1NC-e-Run4), the unbalanced moment transferred from the slab to columns degrades for positive bending as shown in Fig. 12(b). Degradation is characterized by a drop in the unbalanced moment for increasing slab curvatures during the cycle to peak unbalanced moment, as well as by noting that the unbalanced moment transfer is reduced for the subsequent cycles to the same slab curvature for both positive and negative moment transfer. The approach outlined here was used to assess drift ratios for punching failures for all connections. More information is available in the report by Kang and Wallace [15].

Drift Capacity at Punching

Relationships for drift capacity at punching versus gravity shear ratio are commonly derived (e.g., Moehle [6], Robertson et al. [7]). As noted in the introduction, a fairly significant database of tests exists for isolated RC specimens subjected to quasi-static, cyclic lateral loading. Data for PT tests and tests with shear reinforcement are less abundant. Top or inter-story drift ratios at punching failure were derived from the test data (Kang and Wallace [15]) as indicated in the prior paragraph. Results obtained are compared to the existing database of reinforced concrete slab-column connections with and without shear reinforcement (Fig. 13) to assess whether existing trends are appropriate for the dynamic tests of the RC and PT specimens with shear reinforcement. The data plotted are based on actual material properties and for a capacity reduction factor $\phi = 1$. Details of the database used are presented by Kang and Wallace [15].

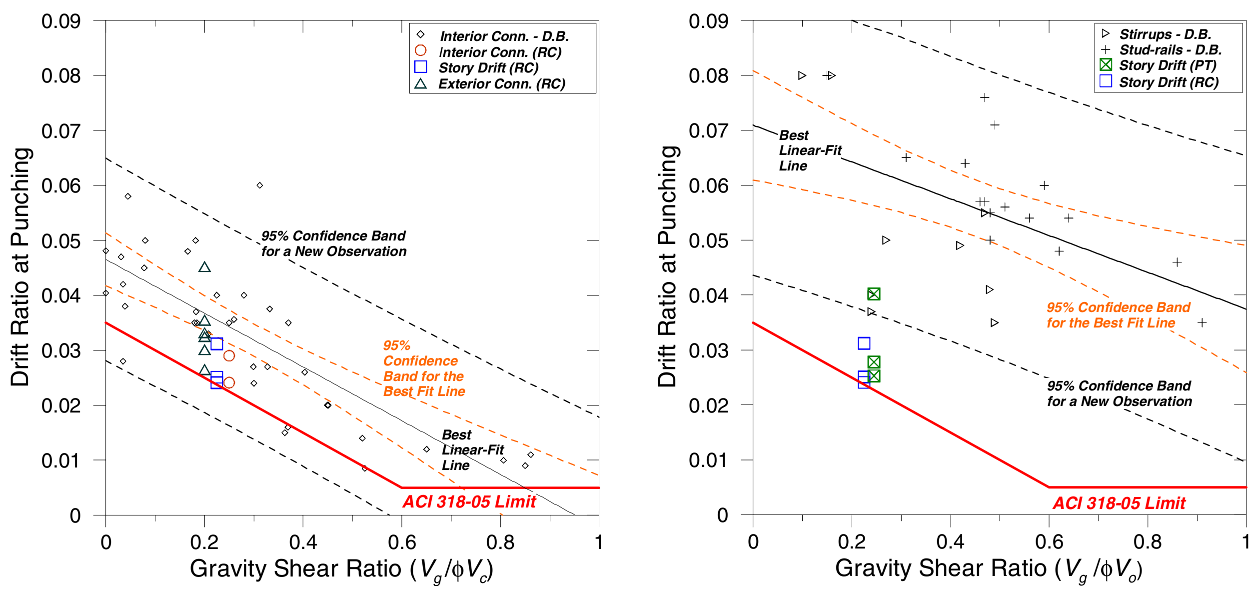

(a) RC slabs w/o shear reinforcement. **(b) RC slabs w/ shear reinforcement.**

Figure 13 Gravity shear versus drift ratio.

Several significant trends are apparent in the results presented in Fig. 13. First, for the results presented in Fig. 13(a) for RC specimens without shear reinforcement, a very clear trend exists for the data, with lower drift capacity at punching as the gravity shear ratio increases. Although data for exterior connection tests are sparse, the drift values at punching and the scatter for the results plotted are consistent with the results plotted for interior connections. For the 2005 version of ACI 318, new provisions were adopted for Section 21.11 "*Members not designated as part of the lateral-force-resisting system*" to address punching of slab-column connections. For drift and gravity shear ratios that exceed the ACI limit noted on Fig. 13, which is close to a lower bound estimate for cases where punching will occur, use of shear reinforcement is required unless calculations are made that indicate the connection punching shear capacity is not exceeded. Although the new ACI provisions may not prevent punching failures at slab-column connections in the design earthquake, they are likely to result in connections with less severe, and possibly, more repairable damage (Fig. 14).

Results for tests of RC slab-column connections with shear reinforcement are plotted in Fig. 13(b), which indicate that the drift capacity of isolated specimens tested under quasi-static, monotonic and cyclic displacement histories is substantially increased where shear reinforcement is used (e.g., Robertson et al. [7]). However, drift ratios at punching derived from the shake table tests described in this paper are substantially less than those obtained in prior testing. This result is somewhat surprising. In quasi-static testing, it is fairly common to apply cyclic displacement history to the specimen and hold the test at or near peak displacement values as cracks and damage are noted, and photos taken. Therefore, there is an expectation that the degree and extent of cracking would be more significant for quasi-static tests compared with dynamic tests, where peak displacements occur for only a very short duration, and thus, larger drift capacities would be expected for dynamic tests. Two factors appear to contribute to the trends noted in Fig. 13(b). First, in the shake table tests conducted large strains were not achieved in the stud-rails (max strain: 812μs; yield strain: 2500μs), whereas stud-rail yielding was achieved in many of the other tests depicted in Fig. 13(b). Second, observed connection behavior during the shake table tests (captured on video) suggests that the shear strength at the interface between the slab and the column deteriorated such that the column was free to rotate without causing further damage to the slab. It is likely that this degradation in interface shear capacity would not be captured in quasi-static tests. The drift ratios at punching derived from the shake table tests of the RC and PT specimens are similar to results obtained for the tests of connections without shear reinforcement. Although the findings presented here are preliminary, they suggest that the new provisions for ACI 318-05 are appropriate for both RC and PT construction, with and without shear reinforcement, and essentially represent a lower bound estimate of cases where punching failures are anticipated.

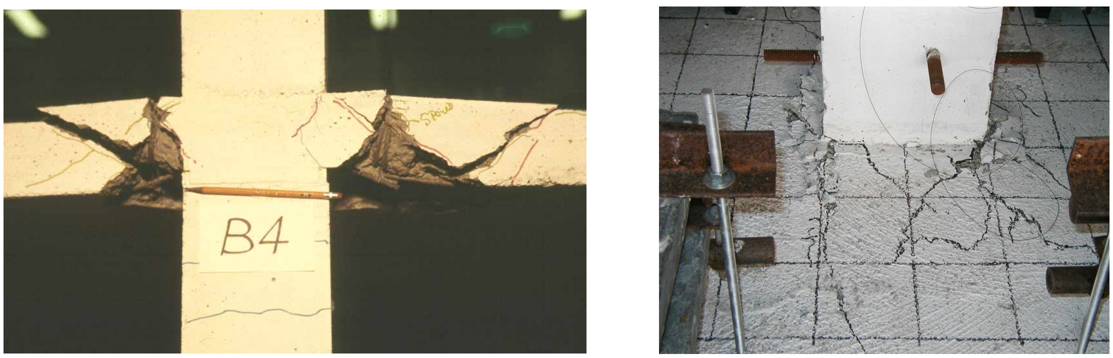

(a) Static tests of RC slabs w/o shear reinforcement. (b) Dynamic tests of PT specimen.

Figure 14 Punching Failure.

Results for the shake table test program involved relatively low gravity shear stress ratios at the connections relative to US practice (because of the dual focus of the research program for both US and Japan practice). Additional tests at higher ratios (e.g., 0.4 to 0.5) would be helpful to verify the trends identified.

CONCLUSIONS

Two, approximately one-third scale slab-column frames were constructed and subjected to dynamic loading on a shake table. An evaluation of measured responses indicates that the moment transfer at the slab-column connections degraded during the tests; however, lateral drift ratios of approximately 3% and 4% were achieved for the RC and PT specimens, respectively, with relatively little loss of lateral load capacity for the system. The tests revealed that use of shear reinforcement (stud-rails) resulted in relatively limited damage to the slab-column connection region compared with tests conducted under slowly varying loads on specimens of similar scale.

Analytical studies were conducted to assess appropriate modification factors to use for effective slab width (α) and cracking (β) for lateral load analysis of slab-column frames. Using an effective slab with model and a column fiber model, α-values of 0.75 and 0.70, and β-values of 1/3 and 2/3, resulted in good correspondence between experimental and analytical results for periods and top displacements, for the RC and PT specimens, respectively. A model capable of capturing the nonlinear behavior of slab-column connections was developed. The model accounted for slab yielding, slab yielding due to unbalanced moment transfer, and punching failures due to either reaching the eccentric shear capacity on the slab critical section or reaching a limiting drift for a specified gravity shear ratio. Comparisons of measured and predicted displacement responses for the PT specimen indicate that the model predictions are very good. Results for the RC test were not as good, although the findings are less reliable due to the lack of footing rotation measurements.

Test results for drift ratios at punching failure versus gravity shear ratios on the slab critical section were evaluated to assess trends for slabs with and without shear reinforcement, as well as new provisions adopted for ACI 318-05. Results for the shake table tests conducted indicate substantially less drift capacity than for prior tests of isolated connections, possibly due to the lower strain demands on the shear reinforcement and the rotation of the slab-column connection due to the apparent loss of interface shear capacity. The relationship between drift and gravity shear ratio adopted in the new ACI provisions is essentially a lower bound estimate of when punching will occur for RC specimens without shear reinforcement, as well as the shake table tests conducted as part of this study.

REFERENCES

1. Pecknold DA. "Slab Effective Width for Equivalent Frame Analysis." ACI Structural Journal 1975; 72(4): 135-137.
2. Moehle JP, Diebold JW. "Experimental Study of the Seismic Response of a Two-Story Flat-Plate Structure." Earthquake Engineering Research Center. Report No. UCB/EERC-84/08, University of California, Berkeley, 1984.
3. "Building Code Requirements for Structural Concrete – ACI 318 (2002)." American Concrete Institute, Farmington Hills, Michigan, 2002.
4. Hawkins NM, Mitchell D. "Progressive Collapse of Flat-Plate Structures." ACI Structural Journal 1979; 76(7): 775-808.
5. Robertson IN, Durrani AJ. "Seismic Response of Connections in Indeterminate Flat-Slab Subassemblies." Report No.41, Department of Civil Engineering, Rice University, 1990.
6. Moehle JP. "Seismic Design Considerations for Flat-Plate Construction." ACI SP-162: Mete A. Sozen Symposium, American Concrete Institute, Farmington Hills, Michigan, 1996: 1-34.
7. Robertson IN, Kawai T, Lee J, Enomoto B. "Cyclic Testing of Slab-Column Connections with Shear Reinforcement." ACI Structural Journal 2002; 99(5): 605-613.
8. Kang THK, Rha C, Wallace JW, Igarashi K, Suzuki N. "Seismic Performance Assessment of Flat Plate Floor Systems." CUREE-Kajima Joint Research Program – Phase IV. Report No. CKIV-02, 2003.
9. Kramer SL. "Geotechnical Earthquake Engineering." Prentice Hall: Upper Saddle River, NJ, 1996.
10. Kang THK. "Shake Table Tests and Analytical Studies of Reinforced Concrete Flat Plate Frames and Post-Tensioned Flat Plate Frames." PhD Thesis, Department of Civil and Environmental Engineering, University of California, Los Angeles, 2004.
11. OpenSees Development Team. "OpenSees: Open System for Earthquake Engineering Simulations." Version 1.5, Berkeley, California, 2002.
12. "NEHRP Guidelines for the Seismic Rehabilitation of Buildings (1997)." Report No. FEMA-274, Federal Emergency Management Agency, October 1997.
13. Allen FH, Darvall P. "Lateral Load Equivalent Frame." ACI Journal 1977; Proceedings, 74(7): 294-299.
14. Kang THK, Wallace JW. "Dynamic Responses of Flat Plate Systems." ACI Structural Journal, submitted for publication, 2004.
15. Kang THK, Wallace JW. "Punching Failure and Drift Capacity at Punching of Reinforced Concrete and Post-Tensioned Slab-Column Connections." ACI Structural Journal, submitted for publication, 2004.
16. Elwood KJ. "Shake Table Tests and Analytical Studies on the Gravity Load Collapse of Reinforced Concrete Frames." PhD Thesis, Department of Civil and Environmental Engineering, University of California, Berkeley, 2002.